Paired electro-oxidation of insecticide imidacloprid and electrodenitrification in simulated and real water matrices

Roger Oriol[1], María del Pilar Bernícola, Enric Brillas[1], Pere L. Cabot[1], Ignasi Sirés*,[1]

Laboratori d'Electroquímica dels Materials i del Medi Ambient, Departament de Química Física, Facultat de Química, Universitat de Barcelona, Martí i Franquès 1-11, 08028 Barcelona, Spain

Paper submitted to be published in ***Electrochimica Acta***

* Corresponding author: Tel.: +34 934039240; fax: +34 934021231.

E-mail address: i.sires@ub.edu (I. Sirés)

[1]Active ISE member

Abstract

Groundwater is one of the main freshwater resources on the Earth, but its contamination by NO_3^- and pesticides jeopardizes its suitability for consumption. In this work, the simultaneous electro-oxidation of insecticide imidacloprid (IMC) and electroreduction of NO_3^- in softened groundwater containing a large amount of Cl^- has been addressed. The assays were carried out in a stirred undivided tank reactor containing either a boron-doped diamond (BDD) or IrO_2 anode, and Fe cathode, which showed greater electrocatalytic activity than stainless steel to reduce NO_3^-. Comparative assays in simulated water mimicking the anionic composition of groundwater were made to assess the influence of natural organic matter (NOM) on the decontamination process. The BDD/Fe cell had much greater performance than the IrO_2/Fe one, although the former produced larger amounts of ClO_3^- and ClO_4^-. In all cases, the NO_3^-, Cl^- and IMC decays agreed with a (pseudo)-first-order kinetics. In the BDD/Fe cell, total NO_3^- removal was reached at $j \geq 10$ mA cm^{-2} in softened groundwater, at similar rate in the presence and absence of IMC, but it was decelerated using the simulated matrix. The N-products formed upon NO_3^- electroreduction contributed to IMC degradation, but its decay was inhibited by NOM because of the partial consumption of oxidants like hydroxyl radical and active chlorine. Operating at 5 mA cm^{-2} for 240 min, total removal of the insecticide and 61.5% total organic carbon (TOC) decay were achieved, also attaining a low NO_3^- content that was suitable for humans. Eight heteroaromatic products were identified, allowing the proposal of a reaction sequence for IMC degradation in groundwater.

Keywords: Boron-doped diamond; Dimensionally stable anode; Electrochemical oxidation; Groundwater; Nitrate removal

1. Introduction

Regions with high density of pig farming and agricultural land are particularly vulnerable to environmental issues linked to groundwater contamination by NO_3^- ion and pesticides. Groundwater is the largest reservoir of liquid freshwater, providing most of the drinking and irrigation water in arid and semiarid areas [1], but the abovementioned pollutants can cause diseases and serious health problems to human beings and animals. The occurrence of NO_3^-, one of the major contaminants of natural water [1,2], is due to: (i) improper disposal of nitrate-laden wastewater, (ii) acid deposition of atmospheric N_xO_y, and (iii) large use of nitrogen fertilizers, including swine wastewater. As a result of its large stability at ambient conditions, NO_3^- is accumulated in water and reaches concentrations as high as 900 mg L^{-1} [1]. Since the excessive intake of dissolved NO_3^- exerts behavioral and cardiovascular diseases, as well as methaemoglobinaemia [3,4], the World Health Organization (WHO) has established a guideline value of 50 mg L^{-1} NO_3^- for human consumption [4]. However, NO_3^- removal from groundwater is difficult because of its high solubility and poor adsorption or precipitation. Hence, this ion is usually treated by reverse osmosis, electrodialysis and ion exchange [4], but these still are non-destructive, expensive and/or ineffective methods.

On the other hand, neonicotinoids are the most widely employed neuro-active insecticides, being applied to many crops and a large plethora of vegetables and fruits [5,6]. They are very harmful to birds, owing to the reduction in insect population, and honeybee colonies. Relatively high concentrations of neonicotinoids have been detected in natural water [5]. Recent EU regulations have banned the use of several of these compounds due to the environmental risks [7,8]. Imidacloprid (IMC, $C_9H_{10}ClN_5O_2$, *N*-[1-[(6-chloro-3-pyridyl)methyl]-4,5-dihydroimidazol-2-yl]nitramide, M = 255.66 g mol^{-1}) has been the most widespread neonicotinoid in agriculture. Its tolerance varies from 0.02 mg kg^{-1} in eggs to 3.0 mg kg^{-1} in hops, causing hepatotoxicity, immunotoxicity, nephrotoxicity and oxidative stress effects in animals [9]. Due to its high resistance to degradation by conventional methods, IMC has been found at concentrations up to 0.36 μg L^{-1} in urban wastewater [10] and 52

57 μg L^{-1} in agricultural water [11]. This molecule contains five N atoms, which worsens the situation
58 if their transformation into stable NO_3^- is promoted during water treatment.

59 Recently, a wide range of electrochemical technologies is being developed for the
60 decontamination of both, natural water and urban and industrial wastewater [12-16]. Separation
61 methods such as electrodialysis and electrocoagulation have been reported for NO_3^- removal [17],
62 although most research efforts have been devoted to its destruction by electroreduction [2,4,13,17-
63 23]. The effectiveness of the latter technique is tightly related to the properties of the cathode material,
64 the solution composition and its pH, the applied current density (*j*) and the cell configuration. Cu-Zn
65 [17], boron-doped diamond (BDD), stainless steel (SS), silicon carbide, graphite and lead [18,19], Cu
66 [20], Fe and Al [21], nano TiO_2 [22,23] and nano zero-valent iron supported on mesoporous carbon
67 [24] have been tested. The electrochemical reduction is aimed to consecutively transform the target
68 ion into NO_2^-, NH_2OH, N_xO_y, N_2 and NH_3, according to the following overall sequence [2,13,18]:

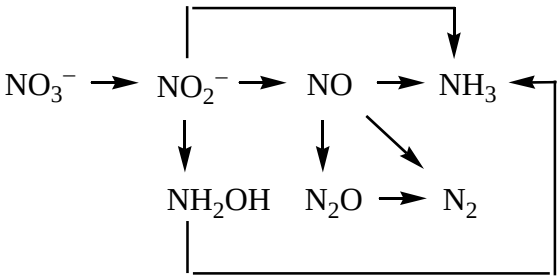

69 (1)

70 In the absence of Cl^- ion, that sequence involves overall reactions (2)-(4) [23]:

71 $NO_3^- + H_2O + 2e^- \rightarrow NO_2^- + 2OH^-$ (2)

72 $NO_2^- + 5H_2O + 6e^- \rightarrow NH_3 + 7OH^-$ (3)

73 $2NO_2^- + 4H_2O + 6e^- \rightarrow N_2 + 8OH^-$ (4)

74 Using undivided reactors, the process is more complicated in the presence of Cl^- ion because
75 active chlorine (Cl_2/HClO/ClO^-) is formed from reactions (5)-(7) [25], further reacting with NH_3 to
76 yield either N_2 by reaction (8) or NO_3^- by reaction (9), or oxidizing NO_2^- to NO_3^- by reaction (10)

[19,20,22], which causes a slower NO_3^- removal. Moreover, chloramines can be originated, for example, from reaction (11), which can evolve either to N_2 or N_2O, as shown by reaction (12) [19].

$$2Cl^- \rightarrow Cl_2(aq) + 2e^- \quad (5)$$

$$Cl_2(aq) + H_2O \rightarrow HClO + H^+ + Cl^- \quad (6)$$

$$HClO \leftrightarrows ClO^- + H^+ \qquad pK_a = 7.53 \quad (7)$$

$$2NH_3 + 2ClO^- \rightarrow N_2 + 2Cl^- + 2H_2O + 2H^+ + 2e^- \quad (8)$$

$$NH_3 + 4ClO^- \rightarrow NO_3^- + H_2O + H^+ + 4Cl^- \quad (9)$$

$$NO_2^- + ClO^- \rightarrow NO_3^- + Cl^- \quad (10)$$

$$NH_3 + ClO^- \rightarrow NH_2Cl + H_2O \quad (11)$$

$$2NH_2Cl + 2ClO^- \rightarrow N_2O + H_2O + 2H^+ + 4Cl^- \quad (12)$$

The anode material may also have influence. Lacasa et al. [19] compared NO_3^- electroreduction in synthetic solutions using either BDD or a dimensionally stable anode (DSA®). The latter anode was very efficient in highly concentrated sulfate medium, whereas BDD performed better in Cl^- medium because the products formed from cathodic NO_3^- reduction were less prone to adsorption on BDD, thereby minimizing their re-oxidation to yield this ion. The electroreduction process is expected to become less efficient in groundwater due to: (i) the presence of CO_3^{2-} that can cause cathode fouling, (ii) the small NO_3^- content, and (iii) the presence of natural organic matter (NOM) [13].

The efficient removal of several pesticides from synthetic solutions by electrochemical advanced oxidation processes (EAOPs) like electro-oxidation (EO), electro-Fenton (EF) and photoelectro-Fenton (PEF) using BDD or DSA® anodes has been reported [26-33]. In contrast, less is known about the treatment of pesticides in groundwater, since as far as we know only the treatment of lindane and IMC has been reported [34,35]. For IMC, EO [14,35-37] and EF [38-40] processes, along with electrocoagulation [41], have been studied in different water matrices.

EO, the simplest EAOP, involves the attack of the strong oxidant hydroxyl radical (M(•OH)) on organic molecules. The radical is originated from water discharge on an active or non-active anode (M) at high *j* from reaction (13) [42,43]. The non-active BDD electrode has been found as the most powerful anode, since it yields large quantities of reactive M(•OH) as compared to DSA® [44]. In Cl^- media, the performance of the latter anode is substantially upgraded because of its higher selectivity to produce active chlorine, which then contributes to the oxidative degradation of organics. However, in some cases, BDD anode possesses higher mineralization power even in such media due to its ability to destroy the chlorinated by-products [44].

$$M + H_2O \rightarrow M(^{\bullet}OH) + H^+ + e^- \quad (13)$$

In this work, the simultaneous IMC electro-oxidation and NO_3^- electroreduction in groundwater is assessed for the first time. This aims at ensuring the electrodenitrification of the aqueous matrix, which is related to the decrease of total nitrogen (TN) content. The assays were performed in an undivided cell equipped with a BDD or IrO_2 (i.e., DSA®-O_2) anode and Fe or stainless steel (SS) cathode. The real groundwater was previously softened to minimize the alkaline earth metal ions and carbonate concentrations, and IMC was spiked into it at 10.0 mg dm^{-3} of total organic carbon (TOC). This high concentration was chosen to monitor the degradation and mineralization and to identify the products formed. Comparative assays with pure and simulated water mimicking the anionic composition of the softened groundwater were also made in order to clarify the raw NO_3^- electroreduction process and the role of NOM.

2. Materials and methods

2.1. Chemicals

Analytical standard imidacloprid (PESTANAL®) was provided by Sigma-Aldrich. Analytical grade NaOH (98-100%) and H_2SO_4 (95-98%) were provided by Panreac. Analytical grade KNO_3

(98%) from Panreac, Na_2SO_4 (99.9%) from BDH PROLABO®, and NaCl (99%) from Panreac were used for the preparation of the simulated water matrix. Carboxylic acids and other chemicals were either of analytical or HPLC grade purchased from Fluka, Merck and Probus. Analytical solutions and the simulated water matrix were prepared with ultrapure water from a Millipore Milli-Q system (resistivity > 18.2 MΩ cm).

2.2. Aqueous matrices

Apart from pure water, the following aqueous matrices were employed to assess the electrodenitrification and EO processes:

(i) A raw groundwater sample, preserved at 4 ºC in a refrigerator once collected from a water well located in an agricultural land in the surroundings of Barcelona (Spain). Its characteristics are shown in Table 1: neutral pH, low conductivity, large amount of HCO_3^- and CO_3^{2-} ions yielding a high total carbon (TC) content, as well as of NO_3^-, Cl^- and SO_4^{2-} ions, and alkaline earth metal ions such as Ca^{2+} and Mg^{2+}. Before electrolytic assays, the raw groundwater was pre-treated following three steps: softening by means of alkalinization up to pH 12 with 20% (w/v) NaOH, filtration to remove the hydroxide and carbonate precipitates formed and, finally, pH adjustment to the original value by adding 10% (v/v) H_2SO_4. As can be seen in Table 1, this softened groundwater showed a drastic reduction of the concentration of all alkaline earth metal ions, whereas the Na^+ and SO_4^{2-} concentrations substantially increased as result of the conditioning procedure. It is also noticeable the low conductivity and TOC of the softened sample, whereas TN mainly corresponded to its NO_3^- content.

(ii) Simulated water prepared to mimic the anions content of the softened groundwater. It was prepared with ultrapure water and contained 2.10 mM KNO_3 (130 mg dm^{-3} NO_3^-), 10.30 mM NaCl (365 mg dm^{-3} Cl^-), and 7.04 mM Na_2SO_4 (690 mg dm^{-3} SO_4^{2-}). The pH was adjusted to 6.8 with 1 M NaOH, thus reaching a conductivity of 1.3 mS cm^{-1}. An analogous solution without NO_3^- was also employed for comparison.

148 *2.3. Electrolytic system*

149 The electrolytic experiments were carried out in a classical two-electrode, cylindrical, jacketed
150 glass tank reactor, which contained 150-175 cm^3 of solution kept under vigorous stirring with a
151 magnetic follower at 800 rpm. The solution temperature was maintained at 25 ºC thanks to the
152 circulation of thermostated water through the jacket. The anode was either a Si wafer coated with a
153 BDD thin film, purchased from NeoCoat (Le-Chaux-de-Fonds, Switzerland), or an IrO_2 electrode
154 purchased from NMT Electrodes (Pinetown, South Africa). The cathode was an iron (Fe, 99.9%) or
155 a SS (AISI 304) plate. All the electrodes had a geometric area of 10 cm^2 in contact with the solution.
156 The two electrodes were placed in the center of the reactor, at 1.5 mm from each other. The assays
157 were performed under galvanostatic conditions with an Amel 2049 potentiostat-galvanostat to
158 provide the constant current density (*j*). The potential difference between the electrodes was directly
159 measured on a Demestres 601BR digital multimeter. The trials with IMC were run after spiking the
160 insecticide at 23.7 mg dm^{-3} (10.0 mg dm^{-3} TOC) into the aqueous matrix.

161 *2.4. Analytical procedures*

162 A Crison 2200 pH-meter was employed to measure the solution pH, and a Metrohm 644
163 conductometer was used for the conductance determination. Active chlorine was measured by the
164 *N*,*N*-diethyl-*p*-phenylenediamine colorimetric method, using an Unicam UV4 UV/Vis
165 spectrophotometer set at λ = 515 nm [45]. A small volume of thiosulfate solution was added to the
166 1.5 cm^3 samples withdrawn from the cell to neutralize the low contents of residual active chlorine,
167 thus ensuring that the degradation process of IMC was stopped. Chloramines were determined upon
168 KI addition, according to the standard 4500-Cl G. DPD Colorimetric Method. All the aliquots were
169 then filtered with Whatman 0.45 μm PTFE membrane filters prior to analysis.

170 Reversed-phase HPLC was used to monitor the IMC concentration. A Waters 600 LC controlled
171 by Empower® software and coupled to a 996 photodiode array detector (PAD) set at λ = 270 nm was
172 utilized. To carry out the analysis, 20 μL aliquots were injected into the LC and the organics were

perfectly separated with a Thermo BDS Hypersil C-18 5 μm (250 mm × 4.6 mm (i.d.)) column at 35 ºC, upon elution with a 50:50 (v/v) acetonitrile/0.02 M phosphate buffer (pH 3) mixture at 1.2 cm^3 min^{-1}. IMC appeared at retention time (t_r) of 3.2 min, with L.O.Q = 0.298 mg dm^{-3} and L.O.D = 0.090 mg dm^{-3}.

The solution TOC was measured on a Shimadzu VCSN TOC analyzer using the non-purgeable organic carbon (NPOC) method. An aliquot volume of 50 μL was injected into it, and reproducible values with ±1% accuracy were always obtained, with L.O.Q = 0.708 mg dm^{-3} and L.O.D = 0.211 mg dm^{-3}. TN measurements were carried out with a TNM-1 unit coupled to the TOC analyzer.

The concentration of Cl^-, ClO_3^-, ClO_4^-, SO_4^{2-}, NO_2^-, NO_3^- and NH_4^+ ions was determined following the analytical procedures previously reported [46]. The content of metal ions was obtained by inductively coupled plasma with optical emission spectroscopy (ICP-OES) using a Perkin Elmer Optima 8300 spectrometer.

Average values obtained in duplicate assays are reported in this work. The corresponding error bars within a 95% confidence interval are shown for the experimental data shown in figures.

Stable heteroaromatic derivatives from IMC degradation were detected by gas chromatography-mass spectrometry (GC-MS), and their mass spectra were compared with those in the NIST05 database. Treated solutions were collected after 60 min of EO treatment of 23.7 mg dm^{-3} insecticide spiked into the softened groundwater matrix, using either a BDD or IrO_2 anode, at 5 mA cm^{-2}. The organics accumulated in each sample were extracted with CH_2Cl_2 (3×15 cm^3) and the organic phase was dried over anhydrous Na_2SO_4, filtered and its volume reduced to about 2 cm^3 under N_2 stream to be analyzed by GC-MS. To do the analysis, the gas chromatograph contained a non-polar Teknokroma Sapiens X5-MS column, and the same procedure previously detailed was applied [47].

3. Results and discussion

3.1. NO_3^- electroreduction in pure water

First, experiments for the selection of the best cathode able to promote the largest NO_3^- electroreduction were carried out. To do this, 150 cm^3 of solutions of 221 mg dm^{-3} NO_3^-, corresponding to 50 mg dm^{-3} N-NO_3^-, in pure water at pH 6.8 after adjustment with H_2SO_4 (i.e., conductivity of 0.88 mS cm^{-1}), was electrolyzed in an undivided reactor with an IrO_2 anode and either Fe or SS cathode at j = 50 mA cm^{-2} for 240 min. At the end of both trials, a slightly greater conductivity of 1.1±0.1 mS cm^{-1} was determined, because of the alkalinization of both solutions to pH near 10.5. This behavior agrees with the reduction of NO_3^- to NO_2^-, NH_3 and N_2 via reactions (2)-(4), which entails an increase of OH^- concentration.

Fig. 1a depicts a gradual decay of N-NO_3^- with electrolysis time, much more rapidly using Fe as the cathode. Average final reductions of 72.8% and 44.0% were obtained using Fe and SS, respectively. A practically constant potential difference between the electrodes (E_{cell}) in each cell was found, with average values of 20.6 V with Fe and 26.1 V with SS. The greater E_{cell} using the SS cathode suggests that the cathode potential became much more negative to maintain the required j, thus informing about its lower catalytic activity towards H_2O and NO_3^- reduction. Fig. 1a also reveals the generation of N-NH_4^+, with maximum values of 9.8 mg dm^{-3} using Fe and 4.6 mg dm^{-3} using SS at 120 min, which were reduced to 4.9 and 0.9 mg dm^{-3}, respectively, at 240 min. The higher N-NH_4^+ production with the Fe cathode agrees with the quicker N-NO_3^- decay, pointing out the higher rate of reaction (3). The drop of N-NH_4^+ concentration at long electrolysis time informs about a gradual re-oxidation of this ion at the IrO_2 anode surface. In addition, the TN dropped down to 21.0 mg dm^{-3} using Fe and 28.9 mg dm^{-3} using SS, corresponding to a nitrogen loss of 57.6% and 42.2% that can be ascribed to the release of volatile N-compounds such as N_2O and, pre-eminently, N_2 [18] (see sequence (1)). Some loss of gaseous NH_3 cannot be discard either because the final pH near 10.5

219 favors its preponderance over soluble NH_4^+ (pK_a = 4.75). Hence, the predominant NO_3^-
220 electroreduction pathway in both systems involves consecutive reactions (2) and (4).

221 From the above results, the speciation of the N-containing species in the resulting electrolyzed
222 solutions was determined, as presented in Fig. 1b. Most of the initial NO_3^- was always converted into
223 volatile products and, to a much lesser extent, into NH_4^+, with greater efficiency using the Fe cathode.
224 In this case, a 5.6% of other undetected species remained in solution, which were not formed using
225 SS. This may be accounted for by the accumulation of products formed from NH_4^+ re-oxidation,
226 which takes place to greater extent with Fe. All these findings confirm the superior electrocatalytic
227 activity of Fe to reduce NO_3^- and hence, this cathode was chosen for all trials described below.

228 *3.2. Fate of nitrogen and chlorine species upon electrolysis in softened groundwater*

229 First electrolyses performed with raw groundwater in BDD/Fe and IrO_2/Fe cells revealed a very
230 low decay of NO_3^- and Cl^-, which was attributed to the passivation of the Fe cathode upon
231 precipitation of carbonates and hydroxides/oxides of highly concentrated alkaline metal ions (Ca^{2+}
232 and Mg^{2+}, see Table 1). To overcome this problem, the raw groundwater was conditioned to remove
233 most of these harmful species, following the procedure described in subsection 2.2. Table 1 shows
234 that the resulting softened groundwater kept the initial TOC (related to NOM) and TN (corresponding
235 to NO_3^-), with a reduction of Cl^- concentration to 365 mg dm^{-3}. The use of this aqueous matrix
236 prevented the cathode passivation in all subsequent electrolyses.

237 The coupling of Fe cathode with a BDD or IrO_2 anode to reach NO_3^- electroreduction alongside
238 Cl^- electro-oxidation was assessed at j values between 5 and 50 mA cm^{-2}. In all these assays, the
239 solution pH remained at circumneutral pH (between 6.8 and 7.8), whereas conductivity remained
240 practically constant as well. No fluctuation of the E_{cell} value was found at each j value tested, always
241 yielding greater potentials in cells with the BDD anode. For example, at j of 5 and 10 mA cm^{-2}, the
242 E_{cell} was of 7.4 and 10.4 V using the BDD/Fe cell, decreasing to 6.1 and 7.7 V using IrO_2/Fe.

Fig. 2a depicts a faster N-NO_3^- decay when *j* rose from 5 to 20 mA cm^{-2} using BDD. After 240 min of electrolysis, the ion was almost completely removed at 10 and 20 mA cm^{-2}, whereas its concentration was only reduced by 81.0% at the lowest *j*. Each N-NO_3^- decay showed an exponential profile, which can be related to a process under mass-transport control. Fig. 2b illustrates the good fitting to a first-order kinetics for the above concentration abatements, which agrees with an analogous finding by Katsounaros et al. [48] using a tin cathode at high potentials. Table 2 shows that the absolute rate constant (k(N-NO_3^-)) was 2.70-fold greater upon a 4-fold increase of *j*, from 5 to 20 mA cm^{-2}. That informs about a gradual loss of the electrocatalytic activity of Fe as *j* was increased, which can be ascribed to the greater extent of H_2 evolution from H_2O reduction. From the TN values measured at the end of these trials, the speciation of the final N-containing species was determined, as shown in Fig. 2c. A progressively higher amount of volatile N-products from 22.0% to 34.4% was observed as *j* was increased, as expected from the acceleration of reaction (4) as well as from N_2 release stimulated via reaction (8) upon the oxidation of NH_4^+ by active chlorine. This is supported by the fact that only a small fraction of NH_4^+, formed from consecutive reactions (2) and (3), was found in these reactions. In all cases, unidentified soluble products accounted for the most of the final TN content. Since no NO_2^- and a very low concentration of chloramines (< 0.05%) were detected, one can conclude that such final products were pre-eminently intermediates originated during the NO_2^- reduction according to scheme (1), alongside species coming from NH_4^+ re-oxidation.

As deduced from Fig. 2d, the oxidation of Cl^- at the BDD anode surface was also gradually enhanced as *j* was increased. The content of this ion was finally reduced by 22.2% at 5 mA cm^{-2}, 66.0% at 10 mA cm^{-2} and 91.2% at 20 mA cm^{-2}. Its exponential decay always obeyed a first-order kinetics (see Fig. 2e), in agreement with a mass-transport controlled process. The rate constants (k(Cl^-)) for these experiments are summarized in Table 2. At each *j* value, k(Cl^-) was lower than k(N-NO_3^-), highlighting the importance of the competition between Cl^- oxidation via reaction (5) and O_2 evolution occurring from the electrochemical oxidation of BDD(•OH), formed via reaction (13), at

the electroactive sites of BDD. For example, a large rise in $k(Cl^-)$, i.e., 4.6-fold, occurred when j was doubled from 5 to 10 mA cm^{-2}, evidencing of a larger enhancement of reaction (5) as compared to O_2 evolution. In contrast, the $k(Cl^-)$ value became exactly twice when j grew from 10 to 20 mA cm^{-2}.

ClO_3^- and ClO_4^- ions were produced at the BDD anode from the consecutive oxidation of ClO^- via reactions (14)-(16) [25,46]:

$$ClO^- + H_2O \rightarrow ClO_2^- + 2H^+ + 2e^- \quad (14)$$

$$ClO_2^- + H_2O \rightarrow ClO_3^- + 2H^+ + 2e^- \quad (15)$$

$$ClO_3^- + H_2O \rightarrow ClO_4^- + 2H^+ + 2e^- \quad (16)$$

Fig. 2f and g show the time course of the ClO_3^- and ClO_4^- contents for the above trials, respectively. Both ions were more largely accumulated at raising j, with predominance of the former one. It is noticeable that almost no ClO_4^- was formed at the lowest j, whereas at the highest j the accumulation of this ion was greatly enhanced from 150 min of electrolysis (see Fig. 2g) at the expense of ClO_3^- (see Fig. 2f). This suggests a remarkable acceleration of reactions (14)-(16) when j is increased. A mass balance at j = 20 mA cm^{-2} reveals that the lost Cl^- was converted into 22.6% of ClO_3^- and 13.7% of ClO_4^-. Since no active chlorine and a very low content of chloramines were found, one can infer that 64% of Cl^- was transformed into gaseous Cl_2.

A lower performance was found for the IrO_2/Fe cell and hence, the electrolyses with the softened groundwater were made up to j = 50 mA cm^{-2}. Fig. 3a shows a poor N-NO_3^- abatement, which increased from 45.9% to 62.2% at 240 min as j was raised from 5 to 20 mA cm^{-2}. Further increase to 30 and 50 mA cm^{-2} yielded decreasing abatements of 59.5% and 53.7%, respectively. Note that the latter value is much lower than that obtained in ultrapure water (see Fig. 1a). The above trend was corroborated from the k(N-NO_3^-) values (see Table 2) determined from the excellent linear plots found for the corresponding first-order kinetic analysis presented in Fig. 3b. As compared to 20 mA cm^{-2}, Table 2 highlights a slightly greater k(N-NO_3^-) value at 30 mA cm^{2} or a similar one at 50 mA

292 cm^2, in agreement with the N-NO_3^- decay trends of Fig. 3a that show a more pronounced deceleration
293 from 60 min at the two highest *j* values. After comparison with the higher rate constants obtained
294 with the BDD/Fe cell (see Table 2), one can conclude that the NO_3^- electroreduction was much less
295 effective using the IrO_2/Fe cell. This can be related to the expected greater production of active
296 chlorine when the IrO_2 anode is employed. Chlorine promotes the oxidation of NH_4^+ to N_2 via reaction
297 (8), alongside the re-oxidation of this ion and NO_2^- to NO_3^- via reactions (9) and (10), respectively.
298 As a result, the overall NO_3^- electroreduction was decelerated, as shown in Fig. 3a. A complementary
299 explanation could be given taking into account the larger ability of IrO_2 to adsorb electroactive species
300 [12,42,43], such as NH_4^+ or NO_2^-, thus favoring their partial conversion into NO_3^-. NO_3^-
301 electroreduction is also slowed down by the competitive reduction of H_2O to H_2, which is expected
302 to be relatively more significant at higher *j*. The production of N-volatiles upon the action of active
303 chlorine, as shown in reaction (8), has been well proven in the literature [19,49]. This aspect was
304 corroborated by determining the speciation of N-containing species at the end of the above assays,
305 on the basis of the TN measured and the absence of NH_4^+, NO_2^- and chloramines in the final solutions.
306 Fig. 3c shows the formation of progressively higher amounts of volatile compounds with increasing
307 *j* from 5 to 30 mA cm^{-2}, being much greater than those determined using the BDD/Fe cell (see Fig.
308 2c). This agrees with the different production of active chlorine in each system, along with the higher
309 accumulation as *j* was upgraded (see below). Furthermore, the decreasing percentage of undetected
310 soluble N-containing compounds with raising *j*, accumulated to much lesser extent as compared to
311 the BDD/Fe cell (see Fig. 2c), suggests that they were intermediates with larger tendency to be
312 transformed into volatiles. Formation of N_2 via reactions (4) and (8), alongside other volatiles, then
313 seems the pre-eminent route for NO_3^- electroreduction using the IrO_2/Fe cell.

314 Regarding the fate of Cl^-, Fig. 3d shows a slow removal of this ion with electrolysis time, which
315 was enhanced from 17.8% at 5 mA cm^{-2} to 46.3% at 30 mA cm^{-2} in 240 min, without further
316 acceleration at 50 mA cm^{-2}. Fig. 3e highlights that the concentration decays always obeyed a first-

317 order kinetics, although with $k(Cl^-)$ values much lower than those found with the BDD/Fe cell (see
318 Table 2), particularly at $j \geq 20$ mA cm^{-2}. Fig. 3f reveals the formation of small quantities of ClO_3^- at
319 the two higher j values, whereas no ClO_4^- was detected in solution, in agreement with results reported
320 elsewhere [19]. The lower oxidation power of the IrO_2 anode as compared to BDD can justify the
321 smaller ability of the IrO_2/Fe cell to remove Cl^-. This active anode has higher electroactivity to
322 convert $IrO_2(^{\bullet}OH)$ formed from reaction (13) into O_2, which strongly reduces the extent of Cl^-
323 oxidation as well as the subsequent destruction of active chlorine via reactions (14)-(16), eventually
324 yielding low amounts of ClO_3^-. The above results described for the N-NO_3^- evolution in this cell
325 suggest that most active chlorine is accumulated as ClO^-, which converts the N-species via reactions
326 (8)-(10). In these reactions, Cl^- is regenerated, impeding its fast removal from the solution. Reactions
327 (8)-(10) occur to much lesser extent using the BDD anode because active chlorine is much more
328 rapidly transformed into ClO_3^- and ClO_4^- ions.

329 *3.3. Paired imidacloprid electrochemical oxidation and NO_3^- electroreduction in simulated water*

330 Once clarified the electrochemical behavior of NO_3^- and Cl^- in the softened groundwater matrix,
331 we focus our efforts on the simultaneous EO of IMC. The paired electrolyses were performed in three
332 different matrices: (i) simulated water with the same anionic composition as the softened
333 groundwater, aiming to avoid the influence of NOM, (ii) the same matrix but without NO_3^-, in order
334 to assess the influence of N-containing species over IMC destruction, and (iii) softened groundwater
335 matrix. All the assays were carried out by spiking 23.7 mg dm^{-3} insecticide (10.0 mg dm^{-3} TOC) into
336 each aqueous matrix at pH 6.8, by applying j values ranging between 5 and 50 mA cm^{-2} using the
337 BDD/Fe and IrO_2/Fe cells. In these experiments, similar trends for pH, conductivity and E_{cell} as those
338 described for the electrolyses without IMC (subsection 3.2) were found.

339 Fig. 4a shows the quicker abatement of IMC when increasing from 5 to 50 mA cm^{-2} using the
340 BDD anode, as a result of its destruction with greater amounts of $BDD(^{\bullet}OH)$ formed from reaction

(13) and active chlorine generated from reactions (5)-(7). Total removal was achieved at gradually shorter times, decreasing from 150 to 60 min. Fig. 4b depicts that the concentration decays followed a pseudo-first-order reaction kinetics, as expected for a mass-transport controlled process like EO in which a steady content of oxidants is produced, thus reacting with the insecticide molecules. As can be seen in Table 2, a 3.2-fold increase of the corresponding apparent rate constant (k(IMC)), from 2.34×10^{-2} to 7.40×10^{-2} min^{-1}, was obtained when j changed from 5 to 50 mA cm^{-2}. This suggests a progressively greater concomitant destruction of oxidants due to the acceleration of their parasitic reactions, as for example O_2 evolution from BDD(•OH) oxidation [12,14]. Table 2 also shows that TOC was reduced by 68.2% at 5 mA cm^{-2}, rising up to 89.1% at 50 mA cm^{-2}, which corroborates the remarkable loss of oxidation power. In this case, the production of recalcitrant chloro-derivatives that are hardly destroyed by BDD(•OH) also plays a crucial role regarding the EO efficiency [12].

Fig. 4c shows the effective simultaneous NO_3^- electroreduction that occurs during the above assays, with N-NO_3^- decays increasing as: 69.7% at 5 mA cm^{-2}, 72.5% at 20 mA cm^{-2} and 97.9% at 50 mA cm^{-2}, after 240 min of electrolysis. The results collected in Table 2 allow inferring the smaller k(N-NO_3^-) values obtained in this simulated matrix as compared with those in softened groundwater without insecticide (see also Fig. 2a), despite the feasibility of almost total NO_3^- removal at the highest j value tested. This deceleration of NO_3^- electroreduction could be ascribed with the generation of NO_3^- from the initial N (6.5 mg dm^{-3}) of IMC [39], as well as the re-oxidation of *N*-containing species derived from oxidation products of this insecticide. On the other hand, Fig. 4d confirms the fast reduction of Cl^- in the simulated matrix, completely disappearing after 180 min at 50 mA cm^{-2}. The k(Cl^-) values under these conditions were even greater than in the absence of the insecticide (see Table 2) due to the enhancement of reaction (5) favored by the attack of produced active chlorine over the organic matter. A good proportionality between k(Cl^-) and j can be observed, informing about a similar efficiency for Cl^- removal. Fig. 4e and f reveal a large conversion of active

chlorine into ClO_3^- and ClO_4^-, respectively, except at j = 5 mA cm^{-2} that did not yielded the latter ion. At the highest j of 50 mA cm^{-2}, the initial Cl^- became completely transformed into oxychlorine ions, with 88.8% of ClO_3^- and 11.2% of ClO_4^-, corroborating the high effectiveness of reactions (14)-(16) to remove active chorine.

From these results, energy consumptions of 52.4 kWh (kg IMC)$^{-1}$ and 41.3 kWh (kg NO_3^-) were determined after 240 min at the lowest j, i.e., 5 mA cm^{-2}, using the BDD/Fe cell. These high values can be explained by the great electrode potential of the BDD anode. In such system, the anode and cathode potentials were +5.2 and -1.6 V/Ag|AgCl, respectively, meaning that the ohmic drop associated to the solution resistance only accounted for 0.6 V.

The results of Fig. 5 inform about the much lower performance of the IrO_2/Fe cell for the paired ICM electro-oxidation and NO_3^- removal. Fig. 5a shows the fast removal of IMC concentration with electrolysis time, which increased as j was raised from 5 to 50 mA cm^{-2} and always obeyed a pseudo-first-order kinetics (see Fig. 5b). However, the resulting k(IMC) values were smaller than those found using a BDD anode (see Table 2). This behavior agrees with the expected lower oxidation power of IrO_2($^\bullet$OH) as compared to BDD($^\bullet$OH), despite the aforementioned larger accumulation of active chlorine using the IrO_2 anode. The much smaller oxidation ability of this anode was confirmed by the null or very low mineralization degree achieved at the end of all electrolyses (see Table 2). A deceleration of N-NO_3^- removal in the simulated matrix as compared to that in the softened groundwater without organic matter can be easily deduced by comparing the data of Fig. 3d and 5c, as well as the k(N NO_3^-) values given in Table 2. This phenomenon has been explained for the BDD/Fe cell. Moreover, Fig. 5d and the k(Cl^-) values of Table 2 also evidence the smaller removal of Cl^- in this medium. This can be ascribed to its slower oxidation via reaction (5) due to the competitive oxidation of the insecticide on the electroactive sites of the anode.

3.4. Electrochemical oxidation of imidacloprid in simulated aqueous matrix without NO_3^-

Fig. 6a and b show the decay of an initial concentration of 23.7 mg dm^{-3} IMC, spiked into simulated water with the same anionic composition of the softened wastewater but without NO_3^- content, at pH 6.8, by EO employing the BDD/Fe and IrO_2/Fe cells at *j* values between 5 and 20 mA cm^{-2}, respectively. By comparing these profiles with those obtained in simulated water with NO_3^- (see Fig. 4a and 5a), one can infer a slower insecticide removal in the case of the BDD/Fe cell. Conversely, using the IrO_2 anode, the absence of NO_3^- in the treated matrix allowed a faster IMC removal. These trends can also be established from the comparison of the *k*(IMC) values listed in Table 2 for 5 and 20 mA cm^{-2}. With BDD, the data of this table also highlight lower *k*(Cl^-) values and TOC removals in the absence of NO_3^-. The decrease of the oxidation power of this cell under the latter conditions suggests that, when NO_3^- is present in the medium, some of the *N*-containing species produced upon NO_3^- electroreduction may attack the insecticide and its oxidation products, thus enhancing their removal and the overall mineralization process. Moreover, such N-products also react with active chlorine, accelerating Cl^- reduction from reaction (5). In contrast, when the IrO_2 anode is alternatively utilized, the greater accumulation of active chlorine in the absence of NO_3^- upgrades its oxidative attack onto ICM. The poor reactivity of IrO_2($^\bullet$OH) is thus responsible for the preponderant role of active chlorine during IMC removal with IrO_2. This effect was much less significant with BDD because of the much greater oxidation ability of BDD($^\bullet$OH).

3.5. Paired imidacloprid electrochemical oxidation and NO_3^- electroreduction in softened groundwater

Finally, the treatment of 23.7 mg dm^{-3} IMC was carried out in the softened groundwater (11.8 mg dm^{-3} TOC, which includes IMC and NOM) at pH 6.8 using both electrolytic cells at 5 mA cm^{-2}. This low *j* value was chosen to prevent the formation of toxic ClO_4^- with the BDD anode. Fig. 7a-c show the superior IMC, N-NO_3^- and Cl^- decays obtained with the BDD/Fe cell, reaching the total insecticide removal at 210 min, in agreement with the results described in subsection 3.3 in the

simulated water. Nevertheless, a closer look at Table 2 confirms that the *k*(IMC), *k*(N-NO_3^-) and *k* (Cl^-) values obtained with both cells in the softened groundwater were significantly lower than those in the simulated water. The same feature can be deduced for the percentage of TOC removed using BDD, although a higher amount of TOC, i.e., 7.3 mg dm^{-3} vs. 6.8 mg dm^{-3}, was destroyed in the former medium because of the concomitant NOM mineralization. This was corroborated by the loss of a small quantity of 1.1 mg dm^{-3} TOC (8.9%) when using the IrO_2 anode, which can be ascribed to the partial destruction of the initial NOM content (1.8 mg dm^{-3}). The lower ability of the cells to remove IMC in the softened groundwater can then be related to the parallel oxidation of NOM, which partly consumes the oxidizing M($^\bullet$OH) and active chlorine produced. In the case of BDD, however, the NOM oxidation had a small effect on NO_3^- electroreduction and Cl^- electro-oxidation, as deduced from the analogous *k*(N-NO_3^-) and *k* (Cl^-) values found in softened groundwater without and with the insecticide (see Table 2). In contrast, much smaller *k*(N-NO_3^-) and *k* (Cl^-) values were determined in the presence of IMC using the IrO_2 anode, which can be associated with a great consumption of active chlorine by NOM since the action of IrO_2($^\bullet$OH) was much milder. All these findings allow concluding the good performance of the BDD/Fe cell to ensure the paired IMC electro-oxidation and NO_3^- electroreduction in actual groundwater. A final content of 27.0 mg dm^{-3} NO_3^- was finally reached (see Fig. 7b), lower than the 50 mg dm^{-3} established by the WHO guideline for human consumption. Under these conditions, ClO_3^- was accumulated in the final solutions. attaining 140.5 mg dm^{-3} after 240 min of electrolysis, as shown in Fig. 7d. This accounts for 64.2% of the removed Cl^-.

3.6. Primary oxidation by-products of imidacloprid

Fig. 8 presents a reaction sequence proposed for the initial degradation of IMC (**1**) that includes all the heteroaromatic products detected by GC-MS after 60 min of EO treatment of 23.7 mg dm^{-3} insecticide spiked into the softened groundwater matrix, using a BDD or IrO_2 anode at 5 mA cm^{-2}.

The initial attack of M(•OH) over **1** causes: (i) the release of the terminal –NO_2 group to yield **2** (1-[(6-chloro-3-pyridyl)methyl]imidazolidine-2-imine, *m*/*z* = 209 (^{35}Cl)) and (ii) the loss of the -NH-NO_2 group to form **3** (2-chloro-5-(4,5-dihydroimidazol-1-ylmethyl)-pyridine, *m*/*z* = 195 (^{35}Cl)), whose imidazole group is subsequently opened to produce **4** ((6-chloro-3-pyridyl)methyl)-(2-imino-ethylidene)-amine), *m*/*z* = 182 (^{35}Cl)). The terminal =NH group of compound **2** is then oxidized to a $=N^+=O$ one yielding **5** (1-[(6-chloro-3-pyridyl)methyl]imidazolidine-2-oxime, *m*/*z* = 225 (^{35}Cl)), which undergoes further denitrozation leading to **6** (1-[(6-chloro-3-pyridyl)methyl]imidazolidin-2-one, *m*/*z* = 211 (^{35}Cl)). Compound **6** can also be produced from direct oxidation of compound **2**. The subsequent degradation of these heteroaromatics involves the cleavage of the imidazole group to yield **7** (6-chloronicotinonitrile, *m*/*z* = 138 (^{35}Cl)), whose nitrile group is then converted into a carbaldehyde one to yield **8** (6-chloronicotinoaldehyde, *m*/*z* = 140 (^{35}Cl)). On the other hand, the imidazole group can also be released and oxidized to form **9** (imidazolidine-2,4,5-trione, *m*/*z* = 114). Note that compound **5** has been identified during the IMC treatment in sulfate medium by EO with Pt or BDD and EF with the same anodes and a carbon felt cathode [39], whereas the formation of compound **6** has been reported for the photo-Fenton and TiO_2 photocatalysis treatment of IMC solutions [50,51]. Note that chlorinated by-products were not detected and, in case of formation, they would be gradually degraded in the BDD/Fe cell.

4. Conclusions

The BDD/Fe cell outperformed the IrO_2/Fe one for the paired IMC electro-oxidation and NO_3^- electroreduction in all the aqueous matrices tested. Fe cathode showed greater electrocatalytic activity than SS. The main drawback of cells equipped with BDD anode is the co-generation of ClO_3^- and ClO_4^-, whose concentration may be minimized by working at low *j* values. The NO_3^- and Cl^- decays agreed with a first-order kinetics, whereas IMC removals followed a pseudo-first-order kinetics. By electrolyzing the softened groundwater without insecticide in the BDD/Fe cell, total NO_3^- removal

was already achieved at $j \geq 10$ mA cm^{-2}, with a large conversion into soluble N-compounds and, to lesser extent, into N-volatiles. Similar NO_3^- decays were found in the presence of IMC, indicating that the EO process did not interfere in the electroreduction process. However, a clear influence of NOM was observed, since NO_3^- removal was clearly decelerated in its presence. The decay of 23.7 mg dm^{-3} IMC in the BDD/Fe cell was accelerated in the presence of NO_3^-, since some of the N-products formed from this ion attacked the parent molecule, alongside BDD($^{\bullet}OH$) and active chlorine. The presence of NOM caused a slower IMC removal due to partial consumption of oxidants. Under these conditions and operating at a low j = 5 mA cm^{-2}, ICM was completely removed in 210 min, whereas after 240 min of electrolysis, 61.5% of TOC was removed and NO_3^- concentration was reduced to 27.0 mg dm^{-3}, becoming suitable for human consumption. The EO process generated 140.5 mg dm^{-3} ClO_3^-. A reaction sequence for the initial IMC degradation in softened groundwater has been proposed.

Acknowledgments

The authors thank the financial support from project CTQ2016-78616-R (AEI/FEDER, EU). R. Oriol acknowledges the FPI grant awarded by MINECO (Spain).

References

[1] M. Gutiérrez, R.N. Biagioni, M.T. Alarcón-Herrera, B.A. Rivas-Lucero, An overview of nitrate sources and operating processes in arid and semiarid aquifer systems, Sci. Total Environ. 624 (2018) 1513–1522.

[2] M. Duca, M.T.M. Koper, Powering denitrification: the perspectives of electrocatalytic nitrate reduction, Energy Environ. Sci. 5 (2012) 9726–9742.

[3] M. Zhou, W. Fu, H. Gu, L. Lei, Nitrate removal from groundwater by a novel three-dimensional electrode biofilm reactor, Electrochim. Acta 52 (2007) 6052–6059.

[4] M. Shrimali, K.P. Singh, J. Greeley, New methods of nitrate removal from water, Environ. Poll. 112 (2001) 351–359.

[5] E. Herrero-Hernández, M.S. Rodríguez-Cruz, E. Pose-Juan, S. Sánchez-González, M.S. Andrades, M.J. Sánchez-Martín, Seasonal distribution of herbicide and insecticide residues in the water resources of the vineyard region of La Rioja (Spain), Sci. Total Environ. 609 (2017) 161–171.

[6] M.L. Hladik, S. Bradbury, L.A. Schulte, M. Helmers, C. Witte, D.W. Kolpin, J.D. Garrett, M. Harris, Neonicotinoid insecticide removal by prairie strips in row-cropped watersheds with historical seed coating use, Agric. Ecosyst. Environ. 241 (2017) 160–167.

[7] European Commission, First Watch List for emerging water pollutants, https://ec.europa.eu/jrc/en/news/first-watch-list-emerging-water-pollutants (last access, June 7, 2018).

[8] J.C.G. Sousa, A.R. Ribeiro, M.O. Barbosa, M.F.R. Pereira, A.M.T. Silva, A review on environmental monitoring of water organic pollutants identified by EU guidelines, J. Hazard. Mater. 344 (2018) 146–162.

[9] Komal, A review: immunological and biochemical studies on imidacloprid toxicity, Pharma Innov. 7 (4) (2018) 999–1002.

[10] A.M. Sadaria, R. Sutton, K.D. Moran, J. Teerlink, J.V. Jackson, R.U. Halden, Passage of fiproles and imidacloprid from urban pest control uses through wastewater treatment plants in northern California, USA, Environ. Toxicol. Chem. 36 (2017) 1473–1482.

[11] M.A. Daam, A.C. Santos Pereira, E. Silva, L. Caetano, M.J. Cerejeira, Preliminary aquatic risk assessment of imidacoprid after application in an experimental rice plot, Ecotoxicol. Environ. Saf. 97 (2013) 78–85.

[12] C.A. Martínez-Huitle, M.A. Rodrigo, I. Sirés, O. Scialdone, Single and coupled electrochemical processes and reactors for the abatement of organic water pollutants: a critical review, Chem. Rev. 115 (2015) 13362–13407.

[13] J. Martínez, A. Ortiz, I. Ortiz, State-of-the-art and perspectives of the catalytic and electrocatalytic reduction of aqueous nitrates, Appl. Catal. B: Environ. 207 (2017) 42–59.

[14] F.C. Moreira, R.A.R Boaventura, E. Brillas, V.J.P. Vilar, Electrochemical advanced oxidation processes: a review on their application to synthetic and real wastewaters, Appl. Catal. B: Environ. 202 (2017) 217–261.

[15] N. Flores, E. Brillas, F. Centellas, R.M. Rodríguez, P.L. Cabot, J.A. Garrido, I. Sirés, Treatment of olive oil mill wastewater by single electrocoagulation with different electrodes and sequential electrocoagulation/electrochemical Fenton-based processes, J. Hazard. Mater. 347 (2018) 58–66.

[16] Z. Ye, J.R. Steter, F. Centellas, P.L. Cabot, E. Brillas, I. Sirés, Photoelectro-Fenton as post-treatment for electrocoagulated benzophenone-3-loaded synthetic and urban wastewater, J. Clean. Prod. 208 (2019) 1393–1402.

[17] M. Li, C. Feng, Z. Zhang, X. Lei, R. Chen, Y. Yang, N. Sugiura, Simultaneous reduction of nitrate and oxidation of by-products using electrochemical method, J. Hazard. Mater. 171 (2009) 724–730.

[18] E. Lacasa, P. Cañizares, J. Llanos, M.A. Rodrigo, Effect of the cathode material on the removal of nitrates by electrolysis in non-chloride media, J. Hazard. Mater. 213-214 (2012) 478–484.

[19] E. Lacasa, J. Llanos, P. Cañizares, M.A. Rodrigo, Electrochemical denitrificacion with chlorides using DSA and BDD anodes, Chem. Eng. J. 184 (2012) 66–71.

[20] Y.F. Ning, Y.P. Chen, Y. Shen, Y. Tang, J.S. Guo, F. Fang, S.Y. Liu, Directly determining nitrate under wide pH range condition using a Cu-deposited Ti electrode, J. Electrochem. Soc. 160 (2013) H715–H719.

[21] K. Govindan, M. Noel, R. Mohan, Removal of nitrate ion from water by electrochemical approaches, J. Water Process Eng. 6 (2015) 58–63.

[22] X. Ma, M. Li, C. Feng, W. Hu, L. Wang, X. Liu, Development and reaction mechanism of efficient nano titanium electrode: reconstructed nanostructure and enhanced nitrate removal efficiency, J. Electroanal. Chem. 782 (2016) 270–277.

[23] L. Wang, M. Li, X. Liu, C. Feng, N. Chen, W. Hu, Design and applications of Ti nano-electrode for denitrification of groundwater, Environ. Technol. 38 (2017) 3055–3063.

[24] W. Teng, N. Bai, Y. Liu, Y. Liu, J. Fan, W.-X. Zhang, Selective nitrate reduction to dinitrogen by electrocatalysis on nanoscale iron encapsulated in mesoporous carbon, Environ. Sci. Technol. 52 (2018) 230–236.

[25] J.R. Steter, E. Brillas, I. Sirés, On the selection of the anode material for the electrochemical removal of methylparaben from different aqueous media, Electrochim. Acta 222 (2016) 1464–1474.

[26] I. Sirés, E. Brillas, G. Cerisola, M. Panizza, Comparative depollution of mecoprop aqueous solutions by electrochemical incineration using BDD and PbO_2 as high oxidation power anodes, J. Electroanal. Chem. 613 (2008) 151–159.

[27] N. Borràs, R. Oliver, C. Arias, E. Brillas, Degradation of atrazine by electrochemical advanced oxidation processes using a boron-doped diamond anode, J. Phys. Chem. A 114 (2010) 6613–6621.

[28] A.R.F. Pipi, I. Sirés, A.R. De Andrade, E. Brillas, Application of electrochemical advanced oxidation processes to the mineralization of the herbicide diuron, Chemosphere 109 (2014) 49–55.

[29] F. Gozzi, I. Sirés, A. Thiam, S.C. de Oliveira, A, Machulek Jr., E. Brillas, Treatment of single and mixed pesticide formulations by solar photoelectro-Fenton using a flow plant, Chem. Eng. J. 310 (2017) 503–513.

[30] D.R.V. Guelfi, F. Gozzi, A. Machulek Jr., I. Sirés, E. Brillas, S.C. de Oliveira, Degradation of herbicide S-metolachlor by electrochemical AOPs using a boron-doped diamond anode, Catal. Today 313 (2018) 182–188.

[31] A. Kesraoui, N. Oturan, N. Bellakhal, M.A. Oturan, Remediation of water contaminated with pesticides by indirect electrochemical oxidation process electro-Fenton, J. Adv. Oxid. Technol. 11 (2018) 276–282.

[32] D.R.V. Guelfi, E. Brillas, F. Gozzi, A. Machulek Jr., S.C. de Oliveira, I. Sirés, Influence of electrolysis conditions on the treatment of herbicide bentazon using artificial UVA radiation and sunlight. Identification of oxidation products, J. Environ. Manage. 231 (2019) 213–221.

[33] D.R.V. Guelfi, Z. Ye, F. Gozzi, S.C. de Oliveira, A. Machulek Jr., E. Brillas, I. Sirés, Ensuring the overall combustion of herbicide metribuzin by electrochemical advanced oxidation processes. Study of operation variables, kinetics and degradation routes, Sep. Purif. Technol. 211 (2019) 637–645.

[34] C.M. Dominguez, N. Oturan, A. Romero, A. Santos, M.A. Oturan, Removal of lindane wastes by advanced electrochemical oxidation, Chemosphere 202 (2018) 400–409.

[35] R. Oriol, D. Clematis, E. Brillas, J.L. Cortina, M. Panizza, I. Sirés, Groundwater treatment using a solid polymer electrolyte cell with mesh electrodes, ChemElectroChem 6 (2019) 1235–1243.

[36] M.B. Brahim, H.B. Ammar, R. Abdelhedi, Y. Samet, Electrochemical removal of the insecticide imidacloprid from water on a boron-doped diamond and Ta/PbO_2 anodes using anodic oxidation process, Korean J. Chem. Eng. 33 (2016) 2602–2609.

[37] L.M. Silva, R.P.A. dos Santos, C.C.O. Morais, C.L. Vasconcelos, C.A. Martínez-Huitle, S.S.L. Castro, Anodic oxidation of the insecticide imidacloprid on mixed metal oxide (RuO_2-TiO_2 and IrO_2-RuO_2-TiO_2) anodes, J. Electrochem. Soc. 164 (2017) E489–E495.

[38] H. Zhao, Y. Wang, Y. Wang, T. Cao, G. Zhao, Electro-Fenton oxidation of pesticides with a novel Fe_3O_4@Fe_2O_3/activated carbon aerogel cathode: high activity, wide pH range and catalytic mechanism, Appl. Catal. B: Environ. 125 (2012) 120–127.

[39] M. Turabik, N. Oturan, B. Gözmen, M.A. Oturan, Efficient removal of insecticide "imidacloprid" from water by electrochemical advanced oxidation processes, Environ. Sci. Pollut. Res. 21 (2014) 8387–8397.

[40] H. Zhao, L. Qian, Y. Chen, Q. Wang, G. Zhao, Selective catalytic two-electron O_2 reduction for onsite efficient oxidation reaction in heterogeneous electro-Fenton process, Chem. Eng. J. 332 (2018) 486–498.

[41] M.A. Nasser Ghalwa, B. Nader Farhat, Removal of imidacloprid pesticide by electrocoagulation process using iron and aluminum electrodes, J. Environ. Anal. Chem 2 (2015) 1000154.

[42] B. Marselli, J. Garcia-Gomez, P.A. Michaud, M.A., Rodrigo, C. Comninellis, Electrogeneration of hydroxyl radicals on boron-doped diamond electrodes, J. Electrochem. Soc. 150 (2003) D79–D83.

[43] A. Galia, S. Lanzalaco, M.A. Sabatino, C. Dispenza, O. Scialdone, I. Sirés, Electrochem. Commun. 62 (2016) 64-68.

[44] I. Sirés, E. Brillas, M.A. Oturan, M.A. Rodrigo, M. Panizza, Electrochemical advanced oxidation processes: today and tomorrow. a review, Environ. Sci. Pollut. Res.21 (2014) 8336–8367.

[45] APWA, AWWA, WEF, Standard Methods for the Examination of Water and Wastewater, 21st ed., Method Number 4500-Cl Chlorine (residual)–G. DPD Colorimetric Method, American Public Health Association, Washington D.C., 2005, pp. 4-67 and 4–68.

603 [46] A. Thiam, I. Sirés, J.A. Garrido, R.M. Rodríguez, E. Brillas, Effect of anions on electrochemical
604 degradation of azo dye Carmoisine (Acid Red 14) using a BDD anode and air-diffusion cathode,
605 Sep. Purif. Technol. 140 (2015) 43–52.
606 [47] J.R. Steter, E. Brillas, I. Sirés, Solar photoelectro-Fenton treatment of a mixture of parabens
607 spiked into secondary treated wastewater effluent at low input current, Appl. Catal. B: Envion.
608 224 (2018) 410–418.
609 [48] I. Katsounaros, D. Ipsakis, C. Polatides, G. Kyriacou, Efficient electrochemical reduction of
610 nitrate to nitrogen on tin cathode at very high cathode potentials, Electrochim. Acta. 52 (2006)
611 1329–1338.
612 [49] A. Kapałka,, L. Joss, A. Anglada, C. Comninellis, K.M. Udert, Direct and mediated
613 electrochemical oxidation of ammonia on boron-doped diamond electrode, Electrochem.
614 Commun. 12 (2010) 1714–1717.
615 [50] A. Agüera, E. Almansa, S. Malato, M.I. Maldonado, A.R. Fernández-Alba, Evaluation of
616 photocatalytic degradation of imidacloprid in industrial water by GC-MS and LC-MS, Analysis
617 26 (1998) 245–251.
618 [51] S. Malato, J. Caceres, A. Agüera, M. Mezcua, D. Hernando, J. Vial, A.R. Fernández-Alba,
619 Degradation of imidacloprid in water by photo-Fenton and TiO_2 photocatalysis at a solar pilot
620 plant: a comparative study, Environ. Sci. Technol. 35 (2001) 4359–4366.
621

Figure captions

Fig. 1. (a) N-NO_3^- concentration removal and N-NH_4^+ accumulated content during the electrolysis of 150 cm^3 of 221 mg L^{-1} NO_3^- in ultrapure water using a stirred undivided tank reactor with a 10 cm^2 IrO_2 anode and a 10 cm^2 Fe or SS (AISI 304) cathode at a current density (*j*) of 50 mA cm^{-2} and 25 ºC. (b) Percentage distribution of the nitrogen species at the end of the above trials.

Fig. 2. Effect of current density on the change of the concentrations of (a) N-NO_3^- (129.4 mg dm^{-3} of initial NO_3^-), (d) Cl^- ion (365.0 mg dm^{-3} of initial Cl^-), (f) ClO_3^- ion, and (g) ClO_4^- ion with time during the electrolysis of 175 cm^3 of softened groundwater at pH 6.8 using an undivided tank reactor with a 10 cm^2 BDD anode and a 10 cm^2 Fe cathode at 25 ºC. (b,e) First-order kinetic analysis for the data of plots (a) and (d). (c) Percentage distribution of the nitrogen species at the end of the above trials.

Fig. 3. Influence of current density on the time course of the concentrations of (a) N-NO_3^-, (d) Cl^- ion and (f) ClO_3^- ion under the same conditions as those described in Fig. 2, but using a 10 cm^2 IrO_2 anode. (b,e) First-order kinetic analysis for the data of (a) and (d). (c) Percentage distribution of the nitrogen species at the end of the above trials.

Fig. 4. Effect of current density on the variation of (a) imidacloprid concentration, (b) the corresponding pseudo-first-order kinetics, and the concentrations of (c) N-NO_3^-, (d) Cl^- ion, (e) ClO_3^- ion and (f) ClO_4^- ion with electrolysis time for the electrochemical treatment of 175 cm^3 of 23.7 mg dm^{-3} insecticide in the simulated water matrix at pH 6.8 and 25 ºC using a BDD/Fe cell.

Fig. 5. Influence of current density on the change of (a) imidacloprid concentration, (b) the corresponding pseudo-first-order kinetics, and the concentrations of (c) N-NO_3^- ion and (d) Cl^- ion with electrolysis time under the same conditions of Fig. 4, but using an IrO_2/Fe cell.

Fig. 6. Effect of current density on imidacloprid concentration vs. electrolysis time for the EO treatment of 175 cm^3 of 23.7 mg dm^{-3} insecticide in the simulated water matrix without NO_3^- at pH 6.8 and 25 ºC using a (a) BDD/Fe cell and (b) IrO_2/Fe cell.

Fig. 7. Time course of (a) imidacloprid, (b) N-NO_3^-, (c) Cl^- and (d) ClO_3^- concentrations for the electrochemical treatment, with BDD or IrO_2 anode, of 175 cm^3 of 23.7 mg dm^{-3} insecticide in softened groundwater at pH 6.8, 25 ºC, and j = 5 mA cm^{-2}.

Fig. 8. Reaction sequence for the initial degradation of imidacloprid in softened groundwater. Solid arrows correspond to intermediates found in the BDD/Fe cell, whereas dashed arrows are used for those identified in the IrO_2/Fe cell.

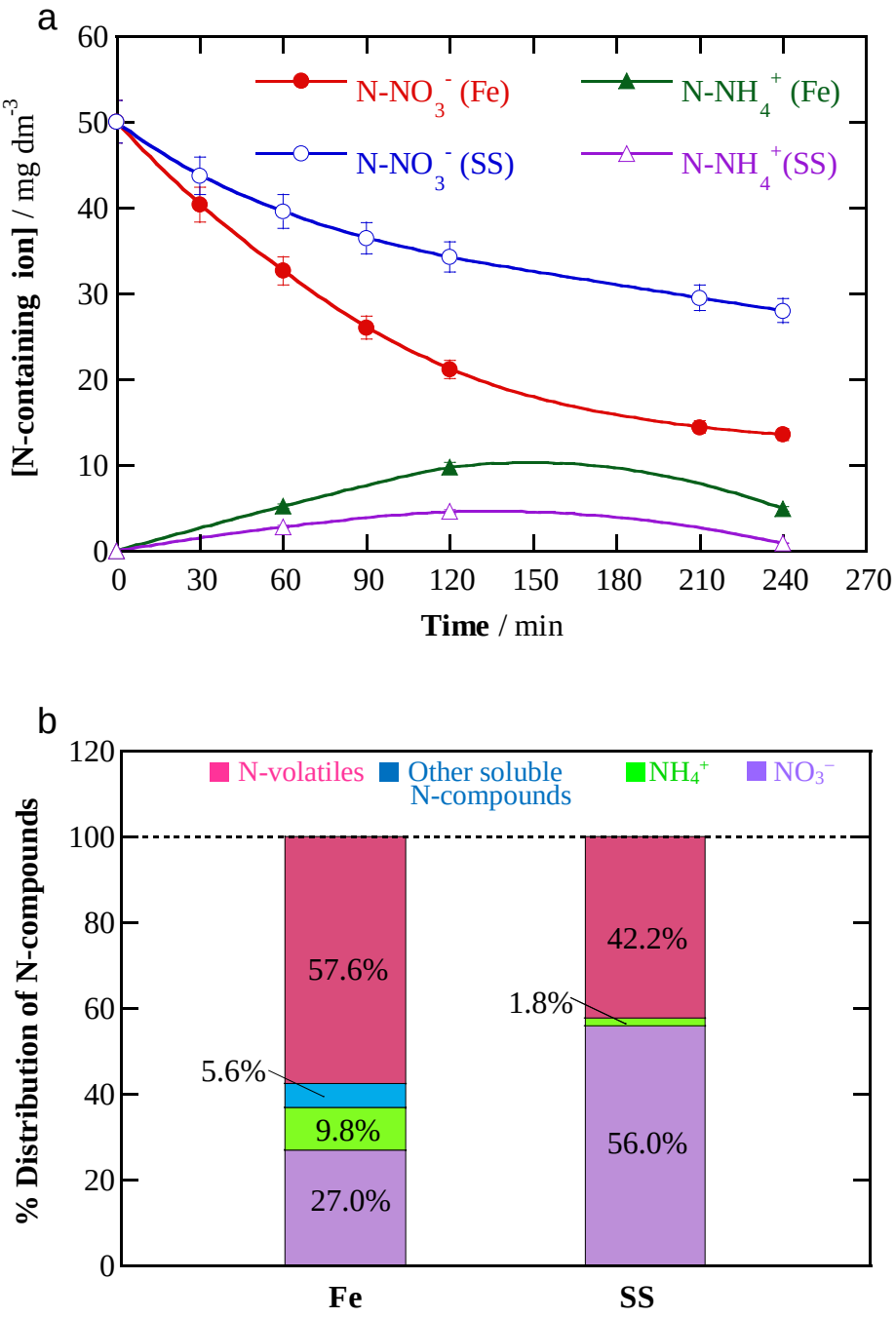
a
[N-containing ion] / mg dm-3
Time / min
N-NO3- (Fe)
N-NH4+ (Fe)
N-NO3- (SS)
N-NH4+ (SS)
0
10
20
30
40
50
60
0
30
60
90
120
150
180
210
240
270
b
% Distribution of N-compounds
N-volatiles
Other soluble N-compounds
NH4+
NO3−
57.6%
5.6%
9.8%
27.0%
42.2%
1.8%
56.0%
Fe
SS

Fig. 1

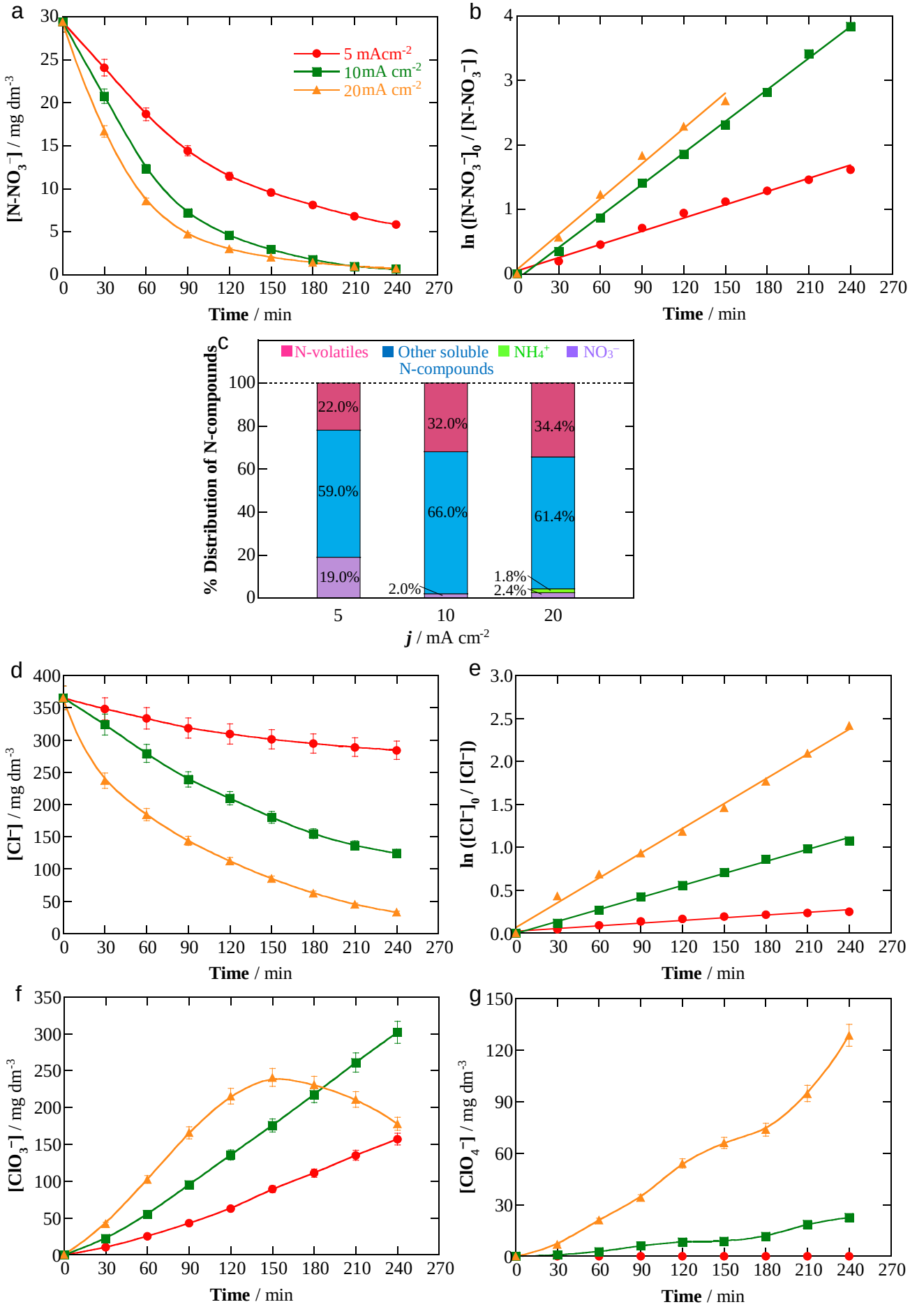
a
[N-NO3−] / mg dm-3
5 mAcm-2
10mA cm-2
20mA cm-2
Time / min
b
ln ([N-NO3−]0 / [N-NO3−])
Time / min
c
% Distribution of N-compounds
N-volatiles
Other soluble N-compounds
NH4+
NO3−
22.0%
59.0%
19.0%
32.0%
66.0%
2.0%
34.4%
61.4%
1.8%
2.4%
j / mA cm-2
d
[Cl−] / mg dm-3
Time / min
e
ln ([Cl−]0 / [Cl−])
Time / min
f
[ClO3−] / mg dm-3
Time / min
g
[ClO4−] / mg dm-3
Time / min

Fig. 2

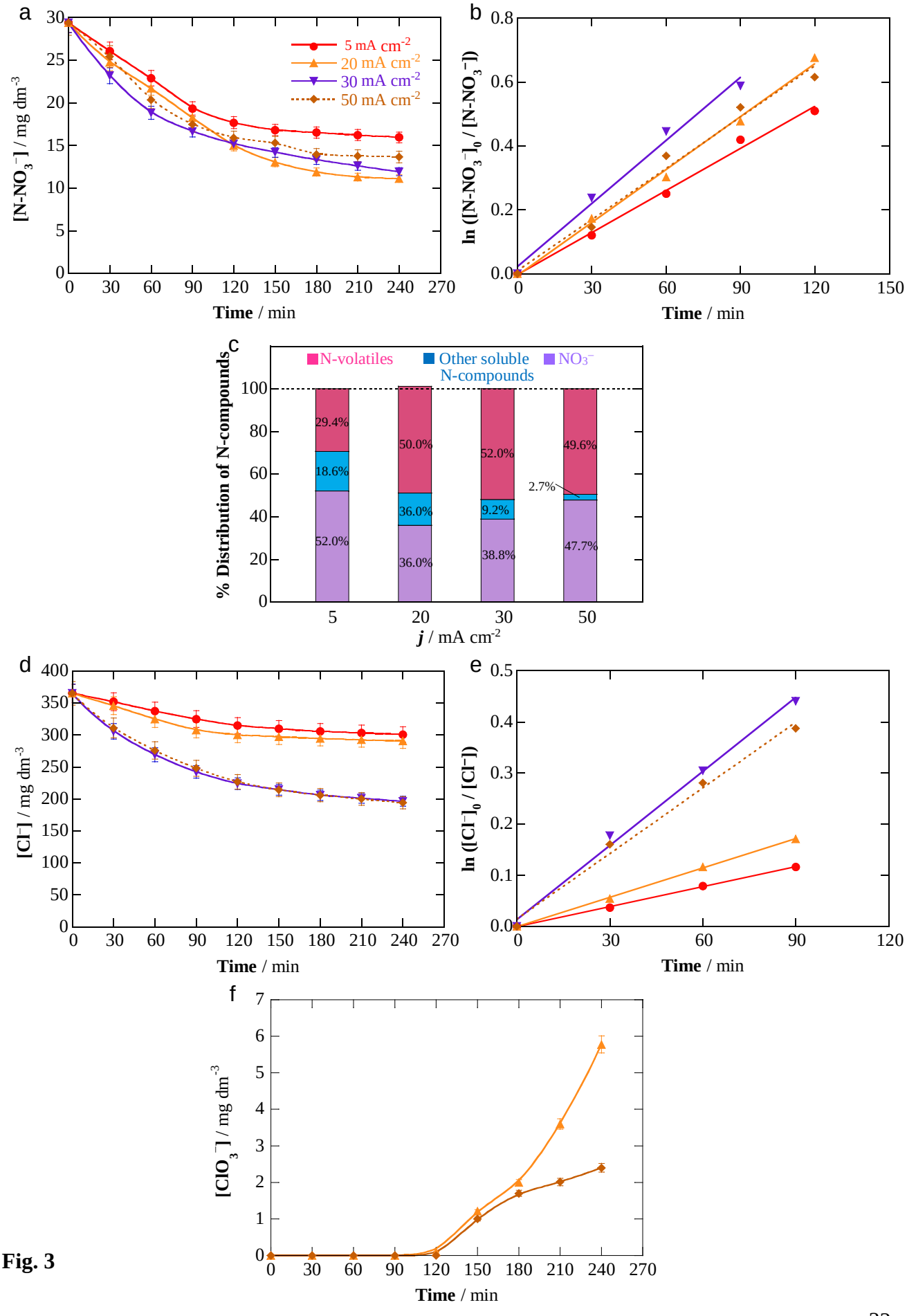
a
[N-NO3−] / mg dm-3
Time / min
5 mA cm-2
20 mA cm-2
30 mA cm-2
50 mA cm-2
b
ln ([N-NO3−]0 / [N-NO3−])
Time / min
c
% Distribution of N-compounds
N-volatiles
Other soluble N-compounds
NO3−
29.4%
18.6%
52.0%
50.0%
36.0%
36.0%
52.0%
9.2%
38.8%
49.6%
2.7%
47.7%
j / mA cm-2
d
[Cl−] / mg dm-3
Time / min
e
ln ([Cl−]0 / [Cl−])
Time / min
f
[ClO3−] / mg dm-3
Time / min

Fig. 3

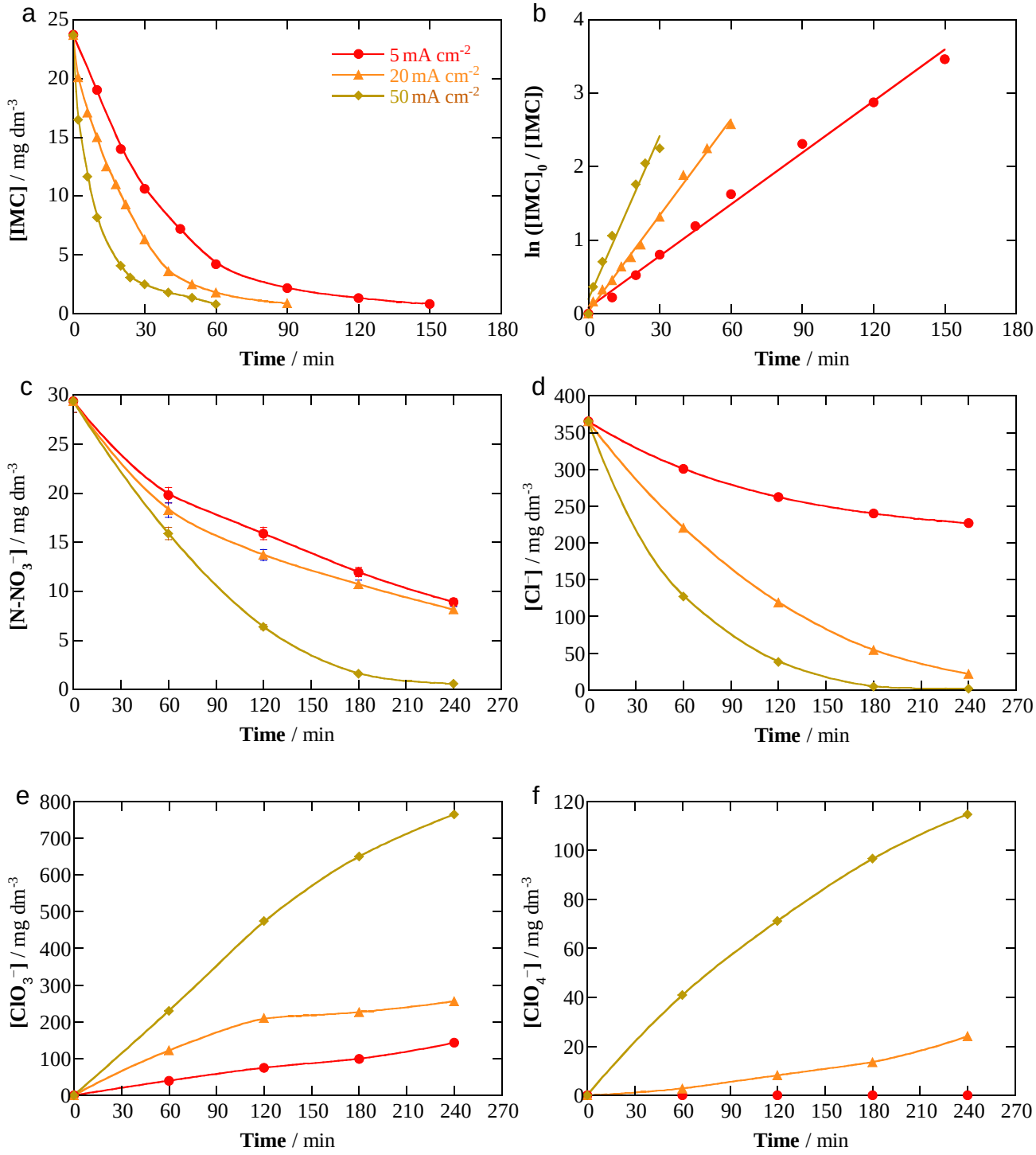
a
[IMC] / mg dm-3
Time / min
5 mA cm-2
20 mA cm-2
50 mA cm-2
b
ln ([IMC]0 / [IMC])
Time / min
c
[N-NO3-] / mg dm-3
Time / min
d
[Cl-] / mg dm-3
Time / min
e
[ClO3-] / mg dm-3
Time / min
f
[ClO4-] / mg dm-3
Time / min

Fig. 4

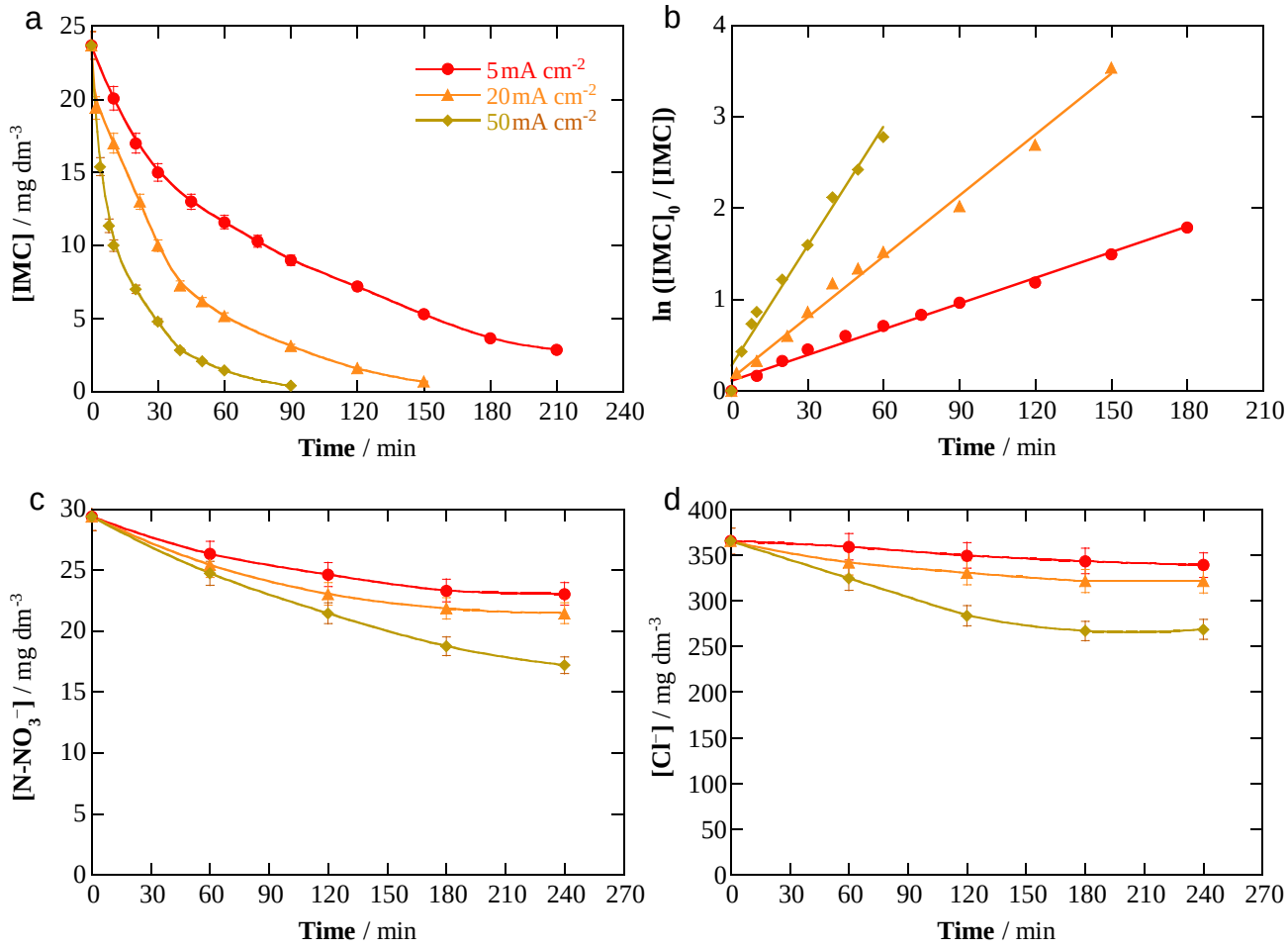
a
[IMC] / mg dm-3
Time / min
5 mA cm-2
20 mA cm-2
50 mA cm-2
b
ln ([IMC]0 / [IMC])
Time / min
c
[N-NO3-] / mg dm-3
Time / min
d
[Cl-] / mg dm-3
Time / min

Fig. 5

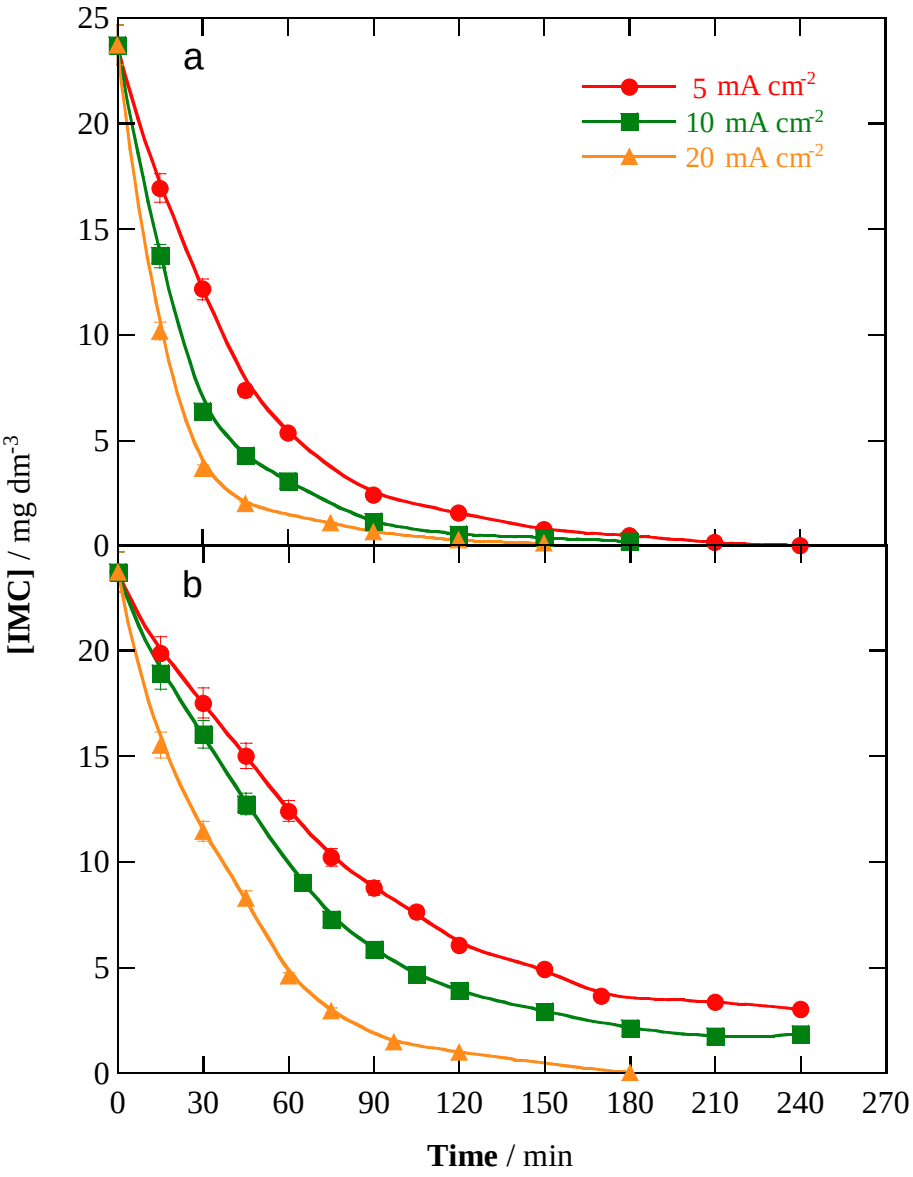
a
b
5 mA cm-2
10 mA cm-2
20 mA cm-2
[IMC] / mg dm-3
Time / min
0
5
10
15
20
25
0
30
60
90
120
150
180
210
240
270

Fig. 6

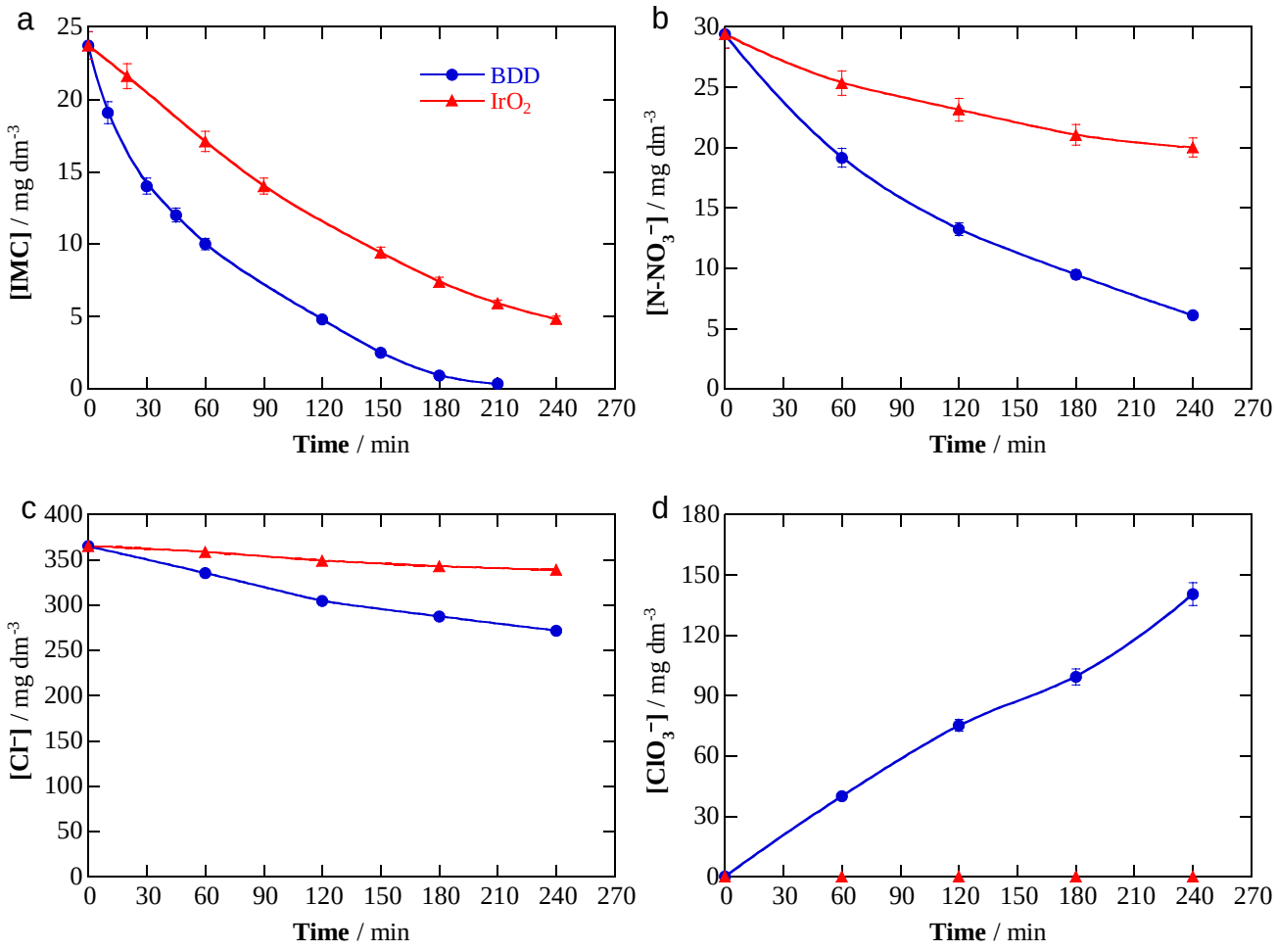
a
[IMC] / mg dm-3
Time / min
BDD
IrO2
b
[N-NO3-] / mg dm-3
Time / min
c
[Cl-] / mg dm-3
Time / min
d
[ClO3-] / mg dm-3
Time / min

Fig. 7

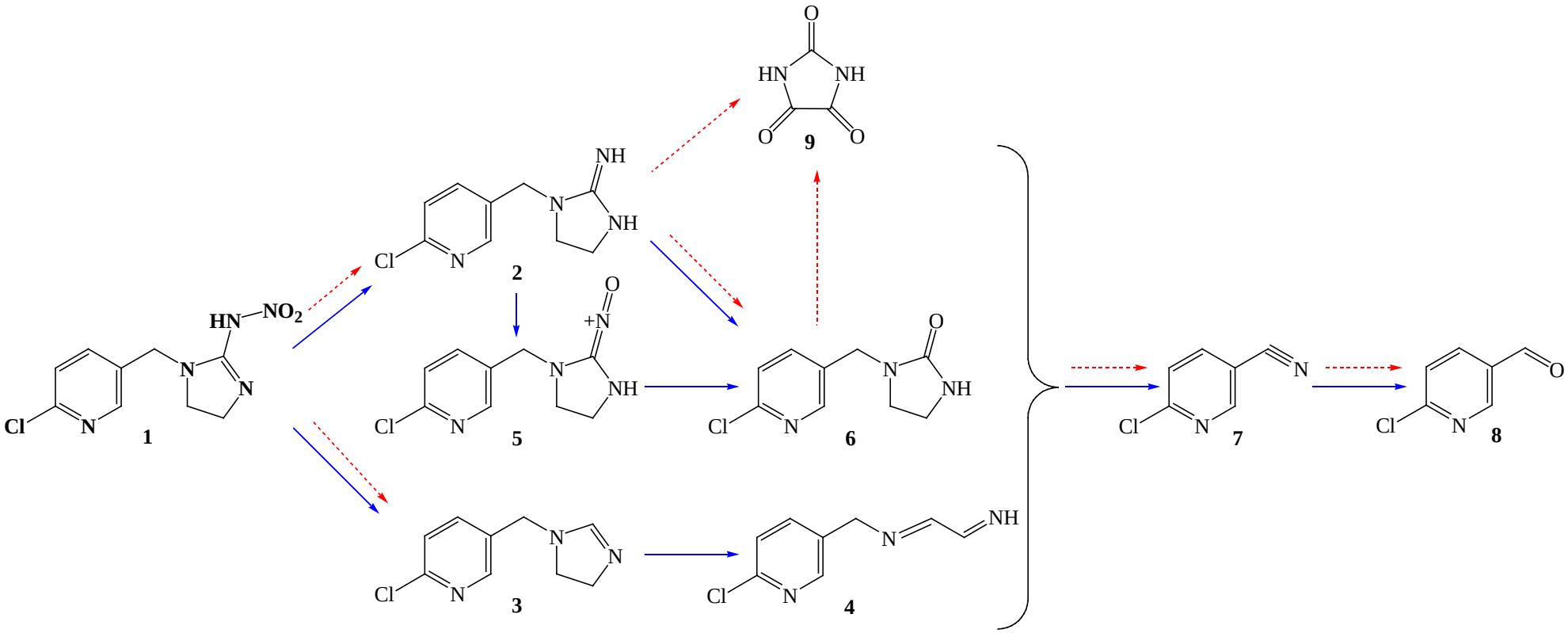

Fig. 8

Table 1

Physicochemical characteristics of the raw and softened groundwater.

Parameter (unit)	Raw groundwater	Softened groundwater
pH	6.9±0.2	6.8±0.3
Conductivity (mS cm^{-1})	0.70±0.03	1.30±0.05
TC (mg dm^{-3})	67.2±2.7	13.1±0.4
TOC (mg dm^{-3})	2.6±0.1	1.8±0.1
TN (mg dm^{-3})	29.2±1.2	29.1±1.1
NO_3^- (mg dm^{-3})	130.0±4.3	129.4±4.8
Cl^- (mg dm^{-3})	366.0±14.4	364.5±17.3
SO_4^{2-} (mg dm^{-3})	88.2±3.8	688.3±28.5
Ca^{2+} (mg dm^{-3})	240.1±9.8	14.4±0.6
Mg^{2+} (mg dm^{-3})	55.4±1.8	0.43±0.02
Ba^{2+} (mg dm^{-3})	0.12±0.01	- [a]
K^+ (mg dm^{-3})	4.1±0.2	3.2±0.1
Na^+ (mg dm^{-3})	80.7±3.2	712.8±26.7
S (mg dm^{-3})	31.6±1.4	288.0±10.5
Si (mg dm^{-3})	11.9±0.4	4.1±0.1

[a] Not found

Table 2

First-order rate constant for N-NO_3^- and Cl^- decays and pseudo-first-order rate constant imidacloprid decay, along with the percentage of TOC removal at the end of the electrolyses. The table includes trials performed with 175 cm^3 of softened groundwater and simulated water matrix, in the presence and absence of the insecticide, at pH 6.8 and 25 ºC using an undivided cell with a BDD or IrO_2 anode and a Fe cathode at different current densities.

Anode	[IMC] / mg dm^{-3}	j / mA cm^{-2}	k(N-NO_3^-) / 10^{-3} min^{-1} (R^2)	k(Cl^-) / 10^{-3} min^{-1} (R^2)	k(IMC) / 10^{-3} min^{-1} (R^2)	% TOC removal at 240 min
Softened groundwater						
BDD	-	5	6.8 (0.992)	1.0 (0.974)	-	-
	23.7	5	6.4 (0.998)	0.9 (0.993)	14.0 (0.991)	61.5 [b]
	-	10	16.3 (0.998)	4.6 (0.998)	-	-
	-	20	18.2 (0.992)	9.6 (0.996)	-	-
IrO_2	-	5	4.4 (0.994)	1.3 (0.999)	-	-
	23.7	5	1.8 (0.985)	0.3 (0.986)	6.7 (0.997)	8.9 [b]
	-	20	5.5 (0.995)	1.9 (0.999)	-	-
	-	30	6.6 (0.988)	4.8 (0.994)	-	-
	-	50	5.3 (0.984)	4.3(0.991)	-	-
Simulated water matrix						
BDD	23.7	5	4.8 (0.993)	2.3 (0.982)	23.4 (0.994)	68.2 [c]
		20	5.2 (0.982)	11.7 (0.986)	43.5 (0.996)	87.3 [c]
		50	16.8 (0.994)	18.8 (0.998)	74.0 (0.980)	89.1 [c]
IrO_2	23.7	5	1.3 (0.983)	0.3 (0.992)	9.4 (0.991)	0 [c]
		20	1.6 (0.980)	0.8 (0.980)	22.2 (0.993)	0 [c]
		50	2.5 (0.996)	1.8 (0.981)	43.5 (0.981)	17.7 [c]
Simulated water without NO_3^-						
BDD	23.7	5	-	0.9 (0.982)	22.1 (0.993)	56.8 [c]
		10	-	- [a]	31.1 (0.988)	60.8 [c]
		20	-	2.1 (0.984)	56.4 (0.992)	71.0 [c]
IrO_2	23.7	5	-	- [a]	11.0 (0.997)	- [a]
		10	-	- [a]	15.0 (0.990)	- [a]
		20	-	- [a]	28.6 (0.992)	- [a]

[a]Not determined; [b]Initial TOC: 11.8 mg dm^{-3}; [c]Initial TOC: 10.0 mg dm^{-3}.